molecules

MDPI

Article

Characterization of Fe_3O_4 Nanoparticles for Applications in Catalytic Activity in the Adsorption/Degradation of Methylene Blue and Esterification

Juan Sebastian Trujillo Hernandez [1,2,*], Alberto Aragón-Muriel [3], Willinton Corrales Quintero [4], Juan Camilo Castro Velásquez [4], Natalia Andrea Salazar-Camacho [4], German Antonio Pérez Alcázar [1,2] and Jesús Anselmo Tabares [1,2]

[1] Grupo de Metalurgia Física y Teoría de Transiciones de Fase, Departamento de Física, Universidad del Valle, Cali 25360, Colombia
[2] Centro de Excelencia de Nuevos Materiales (CENM), Universidad del Valle, Cali 25360, Colombia
[3] Laboratorio de Investigación en Catálisis y Procesos (LICAP), Departamento de Química, Universidad del Valle, Cali 25360, Colombia
[4] Facultad de Ciencias Naturales y Matemáticas, Universidad de Ibagué, Ibagué 730002, Colombia
* Correspondence: juan.sebastian.trujillo@correounivalle.edu.co

Abstract: The aim of this study is to evaluate the applicability of the catalytic activity (CA) of the Fe_3O_4 magnetic system in the adsorption/degradation of methylene blue and esterification. The thermal decomposition method allowed the preparation of Fe_3O_4 nanoparticles. The crystallites of the Fe_3O_4 structural phase present an acicular form confirmed by X-ray diffraction. Transmission electron microscopy results identified the acicular shape and agglomeration of the nanoparticles. Mössbauer spectroscopy showed that the spectrum is composed of five components at room temperature, a hyperfine magnetic field distribution (HMFD), two sextets, a doublet, and a singlet. The presence of the HMFD means that a particle size distribution is present. Fluorescence spectroscopy studied the CA of the nanoparticles with methylene blue and found adsorption/degradation properties of the dye. The catalytic activity of the nanoparticles was evaluated in the esterification reaction by comparing the results in the presence and absence of catalyst for the reaction with isobutanol and octanol, where it is observed that the selectivity for the products MIBP and MNOP is favored in the first three hours of reaction.

Keywords: Fe_3O_4 nanoparticles; catalytic activity; Mössbauer spectroscopy; methylene blue; esterification

check for updates

Citation: Hernandez, J.S.T.; Aragón-Muriel, A.; Corrales Quintero, W.; Castro Velásquez, J.C.; Salazar-Camacho, N.A.; Pérez Alcázar, G.A.; Tabares, J.A. Characterization of Fe_3O_4 Nanoparticles for Applications in Catalytic Activity in the Adsorption/Degradation of Methylene Blue and Esterification. *Molecules* **2022**, *27*, 8976. https://doi.org/10.3390/molecules27248976

Academic Editors: Edgar Mosquera-Vargas and Luis Alfredo Rodríguez

Received: 4 October 2022
Accepted: 9 December 2022
Published: 16 December 2022

Publisher's Note: MDPI stays neutral with regard to jurisdictional claims in published maps and institutional affiliations.

Copyright: © 2022 by the authors. Licensee MDPI, Basel, Switzerland. This article is an open access article distributed under the terms and conditions of the Creative Commons Attribution (CC BY) license (https://creativecommons.org/licenses/by/4.0/).

1. Introduction

Iron oxides are widely distributed in nature and can be easily synthesized in the laboratory [1–5]. There are 16 iron oxides, one of the most common being magnetite (Fe_3O_4), and they can be present in their two aggregation states, as Fe^{+2} and Fe^{+3} forming oxides [6–9]. Most iron oxides are crystalline. Physical and chemical properties depend on variables such as the degree of structural order and size of the crystal [7–10]. Magnetite is an iron oxide noted for its magnetic properties. Magnetite nanoparticles exhibit a large surface area that allows them to be functionalized to make biocompatible products (porous surface) [4–11]. This characteristic makes them especially suitable for a wide range of applications in diverse areas such as biotechnology, environmental, medical, pharmaceutical, catalysts, pigments, gas sensors, optical and electromagnetic devices, decontaminants, and wastewater treatment for dye removal [7–13]. In many chemical synthesis processes, the use of catalysts is necessary to carry out a specific reaction, so both conversion and selectivity are important criteria to evaluate the activity of a catalyst. Among the chemical reactions that use catalysts are esterification reactions where an ester and water are obtained from a carboxylic acid and an alcohol. The use of metal oxide

nanoparticles as catalysts in esterification reactions has been evidenced [11–18], which has generated great interest in developing new alternative materials that can be used as more active and low-cost catalysts. In applications for the removal of contaminants containing iron oxide (Fe_3O_4) nanoparticles, Mössbauer studies have shown that magnetite (Fe_3O_4) spectra taken at room temperature show magnetic (ferromagnetic) behavior represented by two sextets, characteristic of the Fe^{+2} (octahedral sites) and Fe^{+3} (tetrahedral sites) states, for larger particle sizes (greater than 100 nm) [19–21]. However, the spectrum shows a non-magnetic (paramagnetic–superparamagnetic) behavior, represented by a doublet or singlet for particle sizes below a critical size (smaller than 20 nm) [21].

In this work, magnetite nanoparticles were produced from the thermal decomposition method, obtaining a particle size distribution where the magnetic measurements showed a competition between ferromagnetic and superparamagnetic behavior. By means of fluorescence spectroscopy, the catalytic activity in the adsorption/degradation of methylene blue was evidenced. The catalytic activity for the esterification of phthalic anhydride with isobutanol and octanol was also investigated; the nanostructured Fe_3O_4 powders could effectively catalyze the esterification.

2. Results

2.1. Structural Results

Refinement of the XRD results (see Figure 1) shows a spinel structure according to the lattice parameters of magnetite a = b = c = 8.379 Å [10,17,22], indicating an acicular shape of the crystals with parallel and perpendicular crystallite sizes of 79.5 ± 1 Å and 137.2 ± 2 Å, respectively [17]. According to the results obtained by TEM (see Figure 2), a tendency toward agglomeration is present in Fe_3O_4 nanoparticles with grain sizes smaller than 50 nm.

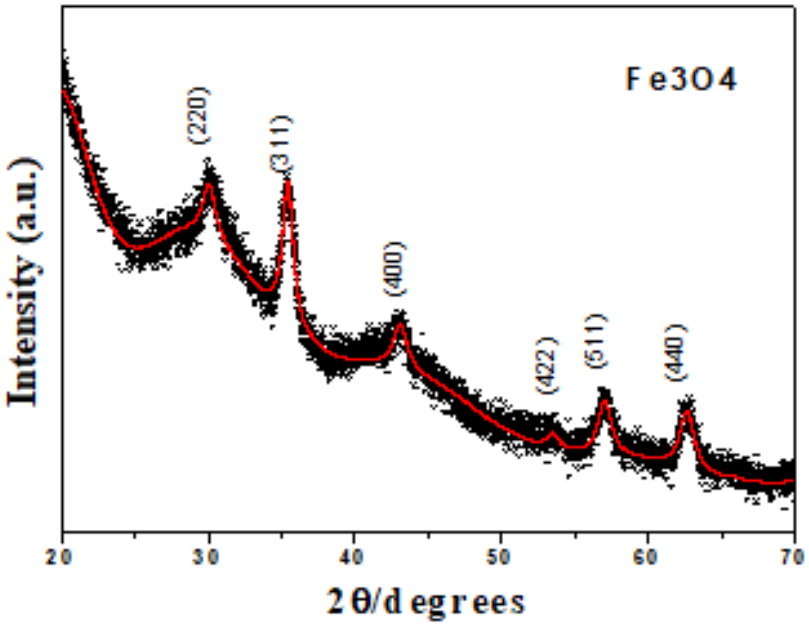


Figure 1. XRD of the Fe_3O_4 system at room temperature [17].

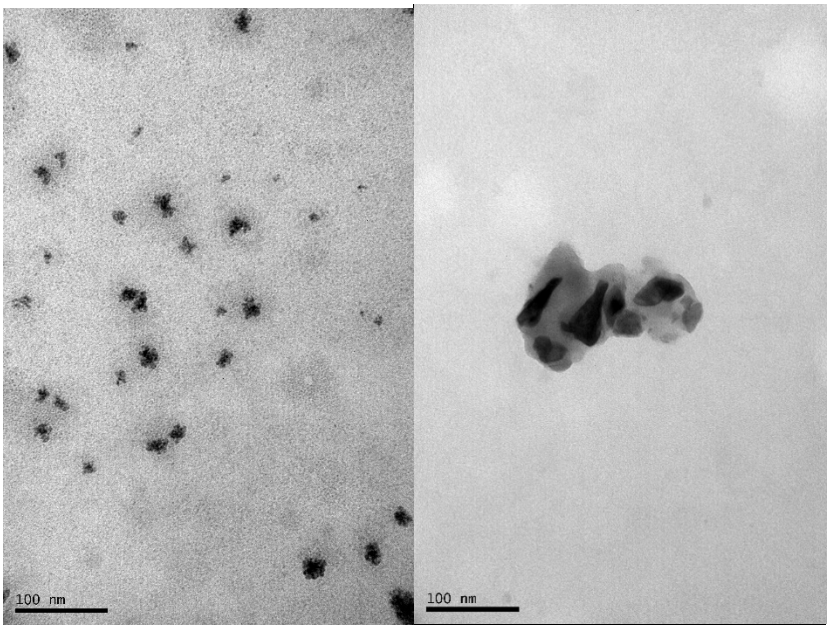


Figure 2. Transmission Electron Microscopy TEM micrograph of Fe_3O_4 agglomerated nanoparticles.

2.2. Mössbauer Results

Figure 3 shows the fit of the Mössbauer spectrum of Fe_3O_4. The fit employed in the spectrum (singlet, doublet, sextet, and a hyperfine magnetic field distribution—HMFD), evidences a particle size distribution given by a HMFD with isomer shift (IS) of -0.22 ± 0.05 mm/s, mean hyperfine field (B_{hf}) of 39.1 $\pm$ 0.2 T, and linewidth (GA) of 0.30 $\pm$ 0.05 mm/s [17,19,20]; the two sextets are associated with iron ions (Fe^{+2} and Fe^{+3}), located at different crystallographic positions within the spinel structure of Fe_3O_4 with IS of 0.41 $\pm$ 0.05 and -0.23 ± 0.05 mm/s, B_{hf} of 39.2 $\pm$ 0.2 and 47.4 $\pm$ 0.2 T. These ionic states at room temperature are not discernible due to their fast electron hopping [17,19,20]. The presence of the two sextets with Mössbauer parameters similar to those reported for the bulk magnetite is attributed to the larger particles. The central part of the spectrum, which contributes the majority of spectral area, is due to the smaller particles, some of which present low hyperfine fields and are near the transition from the superparamagnetic to ferrimagnetic state, and also to those smallest nanoparticles that behave as superparamagnetic and appear as a doublet or singlet [17,21].

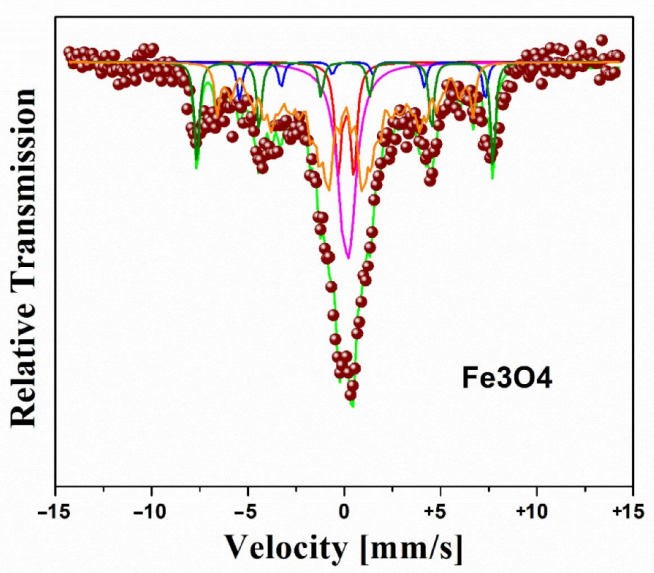


Figure 3. Mössbauer spectra of Fe_3O_4 nanoparticles at room temperature [17].

2.3. FT-IR Spectra

The results obtained by FT-IR are shown in Figure 4. In the spectrum, two strong bands are observed at 669 and 595 cm^{-1}, due to the stretching of the Fe-O (metal–oxygen) bonds by the vibrations in the crystal lattice of Fe_3O_4 [7–9,22–26], characteristically pronounced for ferrites. The octahedral and tetrahedral sites of the oxide are related to these vibration bands. Additionally, hydroxyl groups attached to hydrogen bonds are present in other bands within the spectrum (commonly of the H_2O molecule) [8,9].

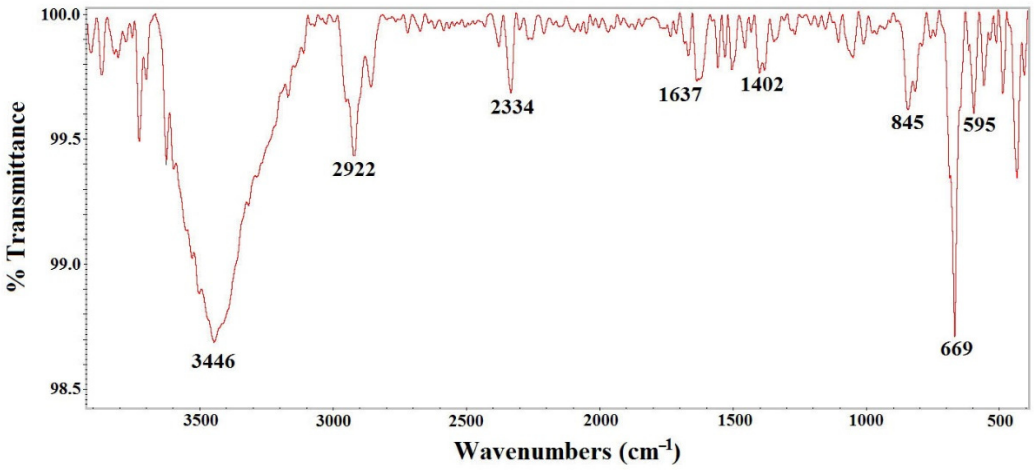


Figure 4. FT-IR spectrum of the Fe_3O_4 nanoparticles.

2.4. Catalysis Studies

The adsorption/degradation rate of MB was obtained by the catalytic activity of the sample in the presence of Fe_3O_4 nanoparticles. To carry out this study over time, it was necessary to choose the optimal dose of nanoparticles, which was achieved by varying the Fe_3O_4/MB ratio in different experiments by UV-Vis spectrophotometry for 1 h of interaction. Figure 5 shows that from 2 mg Fe_3O_4/10 mL MB solution (20 mg/L), there is a significant change in the decrease in absorption corresponding to the presence of the dye; therefore, the following studies were carried out using this dose.

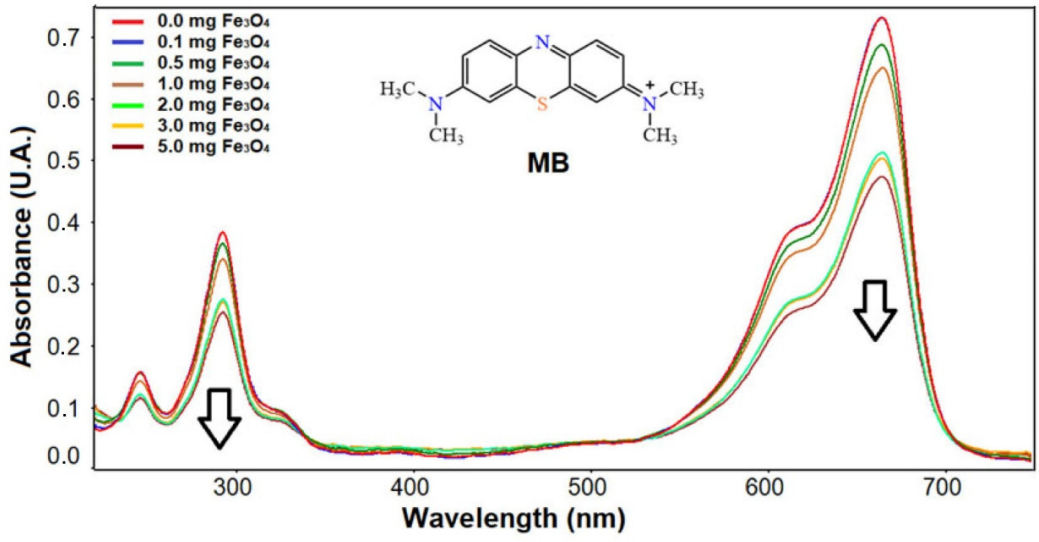


Figure 5. UV-Vis spectra of MB at different doses of Fe_3O_4 nanoparticles after 1 h.

Figure 6 shows at different adsorption times of Fe_3O_4 the degradation of MB at a dose of 2 mg Fe_3O_4/10 mL MB solution. The emission spectra indicated that the concentration

of MB decreases with decreasing emission band at 680 nm, showing unique properties in the adsorption/degradation of this cationic dye with the absorption time of the nanoparticles. Photocatalytic studies with UV irradiation, can increase the catalytic activity of the sample [9,10,25]. Effectively, the nanoparticles showed dye adsorption properties at the time of carrying out the study by fluorescence spectroscopy, since at the beginning a decrease in the concentration of methylene blue was observed without the formation of byproducts (confirmed by mass spectrometry). However, after several minutes of interaction of the nanoparticles with the dye, several methylene blue degradation products were identified in the solution, such as benzenesulfonic acid and thionin, molecules that have been found in other studies of the degradation of methylene blue using mass spectrometry [26], so it can be suggested that the nanoparticles presented both adsorption and catalytic degradation properties.

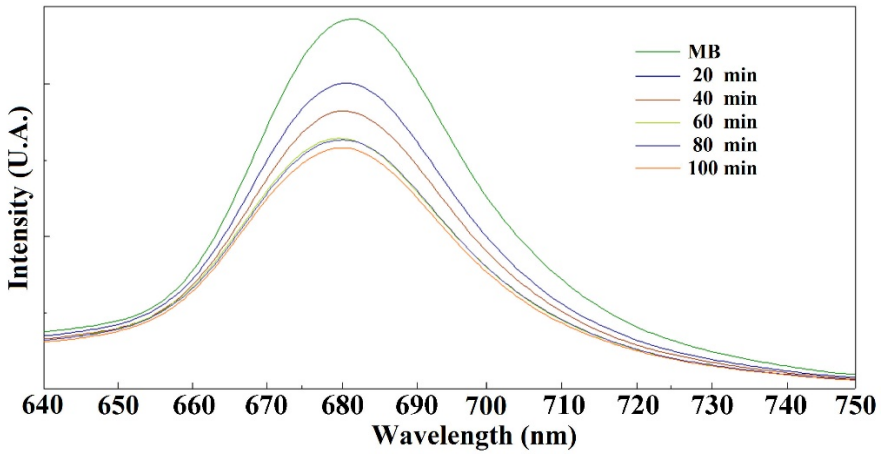


Figure 6. Degradation time in the presence of Fe_3O_4 vs. emission spectra of MB [17].

To understand the adsorption/degradation rate of the dye using synthesized nanoparticles, it was necessary to apply a kinetic model that involves the two simultaneous processes, so it is not recommended to use first- and second- order models or Langmuir–Hinshelwood models for correlation [27,28]. On this occasion, a model similar to the one reported by Giovannetti et al. was used for the adsorption and degradation processes separately [28]. The transformation of MB into adsorbed MB (MB_{Fe3O4}) and into photodegraded products (MB_{PH}) could be treated in terms of two consecutive processes. The first is represented by the decrease in the concentration of MB in the solution due to the adsorption on the surface of Fe_3O_4 nanoparticles. It is shown that the absorption of MB occurs with a process described by the first order kinetic constant k_1 expressed by Equation (1).

$$ln\left[\frac{(q_e - q_t)}{q_t}\right] = -k_1 t \quad (1)$$

where q_t is the amount of dye adsorbed at time t and q_e is the equilibrium concentration [29]. The second process is represented by the photodegradation of MB, a process that occurs with a speed described by the first order kinetic constant k_2 expressed by Equation (2) [29,30].

$$ln\left[\frac{C}{C_0}\right] = -k_2 t \quad (2)$$

where C_0 is the initial concentration of MB and C the concentration of dye at time t.

$$MB + Fe_3O_4 \rightarrow MB_{Fe_3O_4} \qquad k_1$$

$$MB_{Fe_3O_4} + h\nu \rightarrow MB_{PH} \qquad k_2$$

The rate at which MB decreases and the rate for MB_{Fe3O4} and MB_{PH} formation can be expressed as follows:

$$-\frac{d[MB]}{dt} = k_1[MB] \quad (3)$$

$$\frac{d[MB_{Fe_3O_4}]}{dt} = k_1[MB] - k_2[MB_{Fe_3O_4}] \quad (4)$$

$$\frac{d[MB_{PH}]}{dt} = k_2[MB_{Fe_3O_4}] \quad (5)$$

The integration of Equation (3) gives:

$$[MB]_t = [MB]_0 e^{-k_1 t} \quad (6)$$

where $[MB] = [MB]_0$ at time 0, and $[MB] = [MB]_t$ at time t. By substituting Equation (6) into Equation (4), a linear differential equation can be obtained:

$$\frac{d[MB_{Fe_3O_4}]}{dt} = k_1[MB]_0 e^{-k_1 t} - k_2[MB_{Fe_3O_4}] \quad (7)$$

that, after integration, can be written as:

$$[MB_{Fe_3O_4}] = \frac{k_1}{k_2 - k_1}\left(e^{-k_1 t} - e^{-k_2 t}\right)[MB]_0 \quad (8)$$

where $[MB]_0 = [MB] + [MB_{Fe3O4}] + [MB_{PH}]$, so $[MB_{PH}] = [MB]_0 - [MB]_t - [MB_{Fe3O4}]_t$ at time t. Substituting $[MB]_t$ and $[MB_{Fe3O4}]_t$ with Equations (6) and (8), the Equation (9) can be obtained:

$$[MB_{PH}] = \left\{1 + \frac{k_1 e^{-k_2 t} - k_2 e^{-k_1 t}}{k_2 - k_1}\right\}[MB]_0 \quad (9)$$

Using Equations (6) and (9), it was possible to show that the experimental results present a good correlation with the theoretical values of $[MB]_t$ at any time, using concentrations up to 20 mg/L, as shown in Figure 7. The results indicate that as $[MB]_t$ decreases towards low concentrations, the concentration of the intermediate MB_{Fe3O4} (calculated from Equation (8)) rises to a maximum and then decreases towards low concentrations, while the concentration of MB_{PH} (calculated from Equation (9)) increases from the lowest concentration towards $[MB]_0$. With the above, it is shown that the applied model could explain the experimental results and that, from the calculation of $[MB_{Fe3O4}]$ and $[MB_{PH}]$, the evolution of the adsorption/degradation process could be predicted.

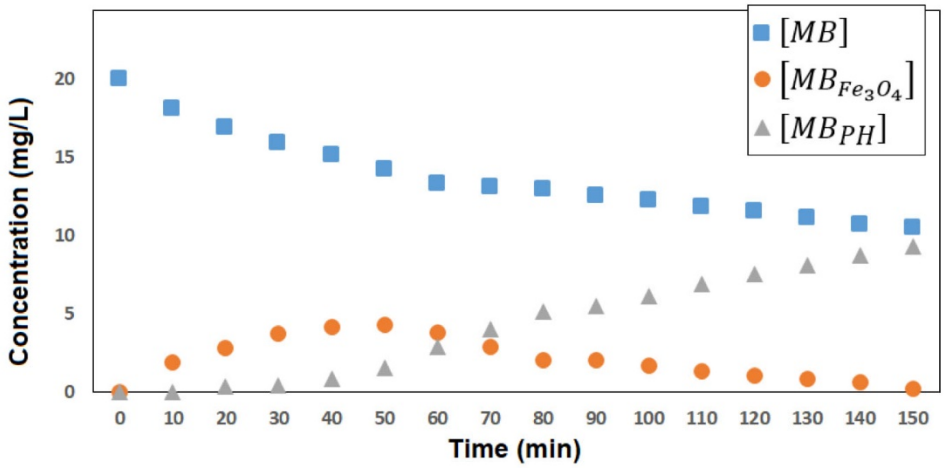


Figure 7. Changes of [MB], $[MB_{Fe3O4}]$, and $[MB_{PH}]$ vs. time in the photodegradation of MB at 20 mg/L catalyzed by Fe_3O_4 nanoparticles.

On the other hand, the esterification of phthalic anhydride with isobutanol and octanol for the synthesis of diisobutyl phthalate (DIBP) and di-n-octylphthalate (DNOP), respectively, was investigated due to its important applications, such as plasticity agents, nail polish, explosive materials, and the lacquer industry [23–26,31]. In the esterification reaction, the chemical reaction shown in Figure 8 occurred, and it was possible to identify the monosubstituted (MIBP, MNOP) and disubstituted (DIBP, DNOP) products.

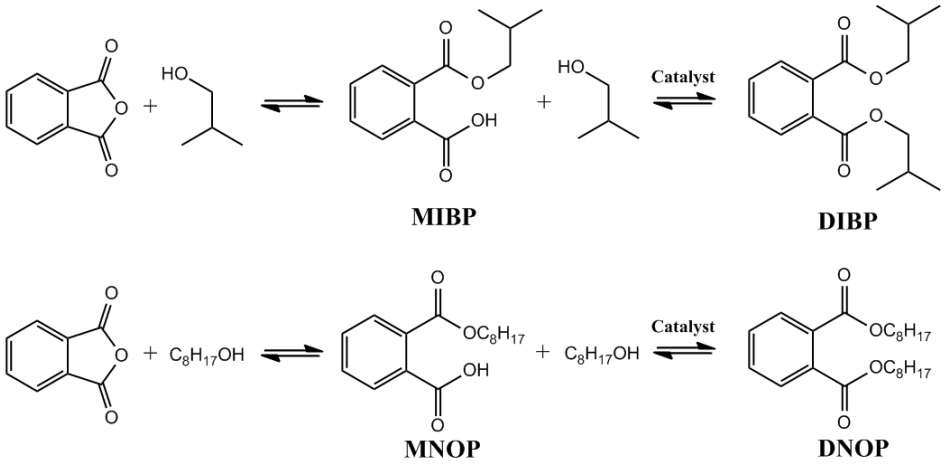


Figure 8. Products obtained in the esterification catalyzed by Fe_3O_4 nanoparticles.

The catalytic activity of the nanoparticles was evaluated in the esterification reaction by comparing the results in the presence and absence of catalyst for the reaction with isobutanol and octanol, as shown in Figures 9a and 10a, respectively. The selectivity for products MIBP and MNOP is favored in the first three hours of reaction, whereas the concentration of DIBP and DNOP products increases as time progresses. In all cases, a slight increase in the conversion to products is observed, so magnetite nanoparticles exhibit activity in this type of reaction, which could increase at different temperatures or different PA:alcohol ratio or by functionalizing the nanoparticles with other materials.

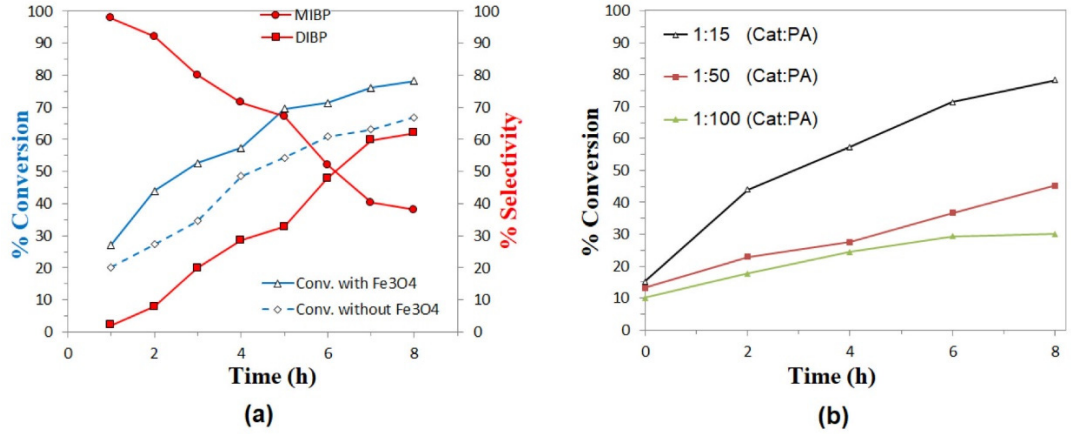


Figure 9. Esterification of phthalic anhydride with isobutanol: (**a**) Conversion of isobutanol and variation in the selectivity of MIBP and DIBP, as a function of time, using Fe_3O_4 nanoparticles as catalysts at 1:15 (catalyst:PA) molar ratio and heated at 120 °C. (**b**) Effect of catalyst:substrate ratio in conversion rates.

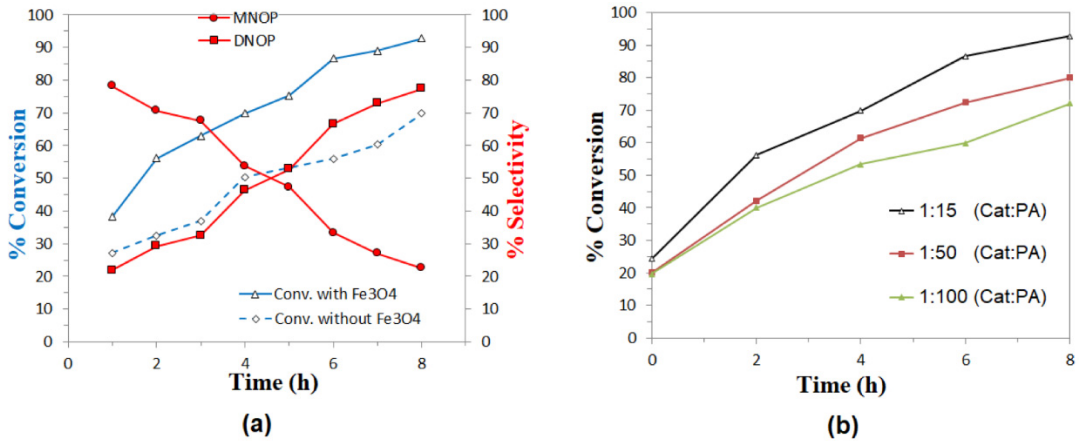


Figure 10. Esterification of phthalic anhydride with octanol: (**a**) Conversion of octanol and variation in the selectivity of MNOP and DNOP, as a function of time, using Fe_3O_4 nanoparticles as catalysts 1:15 (catalyst:PA) molar ratio and heated at 150 °C. (**b**) Effect of catalyst:substrate ratio in conversion rates.

Finally, in evaluating the effect of catalyst concentration, it can be seen in both Figures 9b and 10b that the best results are obtained for the lowest catalyst:substrate ratios (1:15), so it is clear that the higher the catalyst concentration, the higher the reaction percentage in the esterification reactions studied. It is also important to highlight that in the case of the esterification reaction with isobutanol, not much difference is observed for the results at molar ratios 1:50 and 1:100 (Cat:PA), without even exceeding 50% conversion after 8 h, while for the reaction with octanol, all the concentrations evaluated exceed 50% conversion after 6 h of reaction, so it is suggested that these Fe_3O_4 nanoparticles may present better results in the esterification of aliphatic alcohols than longer chain or higher molecular weight alcohols.

3. Experimental Section

Synthesis, Characterization and Catalytic Studies of Fe_3O_4 Nanoparticles

Sodium oleate (5.1 mmol, 1851.2 mg) and iron chloride tetrahydrate [$FeCl_2 \cdot 4H_2O$] (1.4 mmol, 278.3 mg) were stirred in a mixture (280 mL) of water:hexane:ethanol (3:7:4) in a two-necked round bottom flask. The solution was heated for 4 h at 70 °C. The organic layer containing the Fe_3O_4–oleate complex at the end of the reaction was washed with distilled water (30 mL) three times. The hexane was evaporated after washing; the resulting Fe_3O_4–oleate complex was placed in a Pyrex tube and heated for 4 h at 380 °C at a vacuum pressure of 40 Pa. A black fluid was obtained by cooling the reaction mixture to room temperature. To precipitate the produced Fe_3O_4 particles, they were first dispersed in chloroform and dissolved in hexane (20 mL). The particles were isolated by centrifugation and the precipitate appeared upon addition of dispersing agent (chloroform, 0.02 mL). A black solid product was obtained from the precipitate, and this was washed with ethanol and re-dispersed with hexane and finally stored under argon atmosphere. The characterization of the Fe_3O_4 sample was first performed by X-ray diffraction (XRD), using Cu-Kα radiation, and the structural parameters were refined by the Rietveld method, using the GSAS program [32]. Secondly, by Mössbauer spectroscopy (MS), the spectra were adjusted using the MOSFIT program [33], using a ^{57}Co(RH) source in transmission geometry. Thirdly, by transmission electron microscopy (TEM), the morphology of the Fe_3O_4 sample was studied. Fourthly, spectra were obtained by Fourier transform infrared spectroscopy (FTIR), using a NI-COLETT 6700 spectrometer. The electronic absorption spectra were recorded in an UV-visible Evolution 220 Thermo Scientific Spectrophotometer. Finally, using a fluorescence spectrometer (FP-8500, JASCO), the degradation activity of Fe_3O_4 was evaluated using 2 mg of magnetite nanoparticles for every 10 mL of a cationic dye (MB) solution (20 mg/L) for the cationic dye (MB), with the emission band at 680 nm (λexc = 633 nm), keeping adsorption experiments constant at 25.0 ± 0.1 °C and 130 rpm,

The catalytic esterification reactions were carried out in a two-necked flask; phthalic anhydride (650 mg) and Fe_3O_4 nanoparticles (7.5 mg) were added into 2 mL of isobutanol or octanol, and the mixture was heated at 120 and 150 °C, respectively, for several times under stirring. Analysis of the content of the reaction mixtures were made by using a Hewlett Packard 6890 gas chromatograph with a flame ionization detector. The reaction products were identified by mass spectrometry (Shimadzu-GCMS-QP2010) by Electronic Impact ionization at 70 ev.

4. Conclusions

In this work, Fe_3O_4 nanoparticles were prepared by thermal decomposition. The results obtained by Mössbauer for the Fe_3O_4 nanoparticles present the two sextets associated with iron ions (Fe^{+2} and Fe^{+3}) and a particle size distribution given by a HMFD at room temperature. The results obtained by UV-Vis spectrophotometry show that there is a significant change in the decrease in absorption of MB at a dose of 20 mg/L. The emission spectra indicated that the concentration of the cationic dye decreases with decreasing emission band at 680 nm, showing unique properties in the adsorption/degradation with the interaction time of the nanoparticles. According to the kinetic model applied to the adsorption/degradation results, it is suggested that the transformation of MB into adsorbed MB (MB_{Fe3O4}) and into photodegraded products (MB_{PH}) could be treated in terms of two consecutive processes, in which, as time passes, the concentration of MB_{PH} increase while the intermediate product (MB_{Fe3O4}) decreases. The catalytic activity of the nanoparticles was evaluated in the esterification reaction by comparing the results in the presence and absence of catalyst for the reaction with isobutanol and octanol. The selectivity for products MIBP and MNOP is favored in the first three hours of the reaction, whereas the concentrations of the DIBP and DNOP products increase over time. Therefore, the magnetite nanoparticles exhibit activity in this type of reaction.

Author Contributions: Conceptualization, J.S.T.H., A.A.-M. and G.A.P.A.; methodology, J.S.T.H. and J.A.T.; software, W.C.Q. and J.C.C.V.; validation, G.A.P.A., A.A.-M. and N.A.S.-C.; formal analysis, A.A.-M. and J.S.T.H.; investigation, W.C.Q. and J.C.C.V.; resources, N.A.S.-C.; data curation, J.S.T.H.; writing—original draft preparation, A.A.-M., J.S.T.H., G.A.P.A. and J.A.T.; writing—review and editing, G.A.P.A., J.S.T.H. and J.A.T.; visualization, N.A.S.-C.; supervision, G.A.P.A.; project administration, G.A.P.A. and J.A.T.; funding acquisition, J.A.T. All authors have read and agreed to the published version of the manuscript.

Funding: This research was financed by the Research Office of the Universidad del Valle.

Institutional Review Board Statement: Not applicable.

Informed Consent Statement: Not applicable.

Data Availability Statement: The data presented in this study were contained within the article.

Acknowledgments: The authors gratefully acknowledge the financial support to the Research Office of the Universidad de Ibagué and Universidad del Valle.

Conflicts of Interest: The authors declare no conflict of interest.

References

1. Mohajerani, A.; Burnett, L.; Smith, J.V.; Kurmus, H.; Milas, J.; Arulrajah, A.; Horpibulsuk, S.; Kadir, A.A. Nanoparticles in Construction Materials and Other Applications, and Implications of Nanoparticle Use. *Materials* **2019**, *12*, 3052. [CrossRef] [PubMed]
2. Ali, A.; Zafar, H.; Zia, M.; ul Haq, I.; Phull, A.R.; Ali, J.S.; Hussain, A. Synthesis, Characterization, Applications, and Challenges of Iron Oxide Nanoparticles. *Nanotechnol. Sci. Appl.* **2016**, *9*, 49–67. [CrossRef] [PubMed]
3. Andra, S.; Balu, S.K.; Jeevanandham, J.; Muthalagu, M.; Vidyavathy, M.; Chan, Y.S.; Danquah, M.K. Phytosynthesized Metal Oxide Nanoparticles for Pharmaceutical Applications. *Naunyn Schmiedebergs Arch. Pharmacol.* **2019**, *392*, 755–771. [CrossRef] [PubMed]
4. Radoń, A.; Łoński, Y.; Warski, T.; Babilas, R.; Tański, T.; Dudziak, M.; Łukowiec, D. Catalytic Activity of Non-Spherical Shaped Magnetite Nanoparticles in Degradation of Sudan I, Rhodamine B and Methylene Blue Dyes. *Appl. Surf. Sci.* **2019**, *487*, 1018–1025. [CrossRef]

5. Schwaminger, S.P.; Bauer, D.; Fraga-García, P.; Wagner, F.E.; Berensmeier, S. Oxidation of Magnetite Nanoparticles: Impact on Surface and Crystal Properties. *CrystEngComm* **2017**, *19*, 246–255. [CrossRef]
6. Bhole, R.; Gonsalves, D.; Murugesan, G.; Narasimhan, M.K.; Srinivasan, N.R.; Dave, N.; Varadavenkatesan, T.; Vinayagam, R.; Govarthanan, M.; Selvaraj, R. Superparamagnetic Spherical Magnetite Nanoparticles: Synthesis, Characterization and Catalytic Potential. *Appl. Nanosci.* **2022**, *12*, 1–12. [CrossRef]
7. Giraldo, L.; Erto, A.; Moreno-Piraján, J.C. Magnetite Nanoparticles for Removal of Heavy Metals from Aqueous Solutions: Synthesis and Characterization. *Adsorption* **2013**, *19*, 465–475. [CrossRef]
8. Fato, F.P.; Li, D.W.; Zhao, L.J.; Qiu, K.; Long, Y.T. Simultaneous Removal of Multiple Heavy Metal Ions from River Water Using Ultrafine Mesoporous Magnetite Nanoparticles. *ACS Omega* **2019**, *4*, 7543–7549. [CrossRef]
9. Mahdavi, S.; Jalali, M.; Afkhami, A. Removal of Heavy Metals from Aqueous Solutions Using Fe3O 4, ZnO, and CuO Nanoparticles. *J. Nanopart. Res.* **2012**, *14*, 846. [CrossRef]
10. Ali, S.M.; Galal, A.; Atta, N.F.; Shammakh, Y. Toxic Heavy Metal Ions Removal from Wastewater by Nano-Magnetite: Case Study Nile River Water. *Egypt. J. Chem.* **2017**, *60*, 601–612. [CrossRef]
11. Pirsaheb, M.; Moradi, N. A Systematic Review of the Sonophotocatalytic Process for the Decolorization of Dyes in Aqueous Solution: Synergistic Mechanisms, Degradation Pathways, and Process Optimization. *J. Water Process Eng.* **2021**, *44*, 102314. [CrossRef]
12. Panda, S.K.; Prasad, L. Fe_3O_4 Based Nanoparticles as a Catalyst in Degradation of Dyes: A Short Review. *Int. J. Adv. Res. Sci. Commun. Technol.* **2020**, *11*, 34–42. [CrossRef] [PubMed]
13. dos Santos-Durndell, V.C.; Peruzzolo, T.M.; Ucoski, G.M.; Ramos, L.P.; Nakagaki, S. Magnetically Recyclable Nanocatalysts Based on Magnetite: An Environmentally Friendly and Recyclable Catalyst for Esterification Reactions. *Biofuel Res. J.* **2018**, *5*, 806–812. [CrossRef]
14. Nizam, A.; Warrier, V.G.; Devasia, J.; Ganganagappa, N. Magnetic Iron Oxide Nanoparticles Immobilized on Microporous Molecular Sieves as Efficient Porous Catalyst for Photodegradation, Transesterification and Esterification Reactions. *J. Porous Mater.* **2022**, *29*, 119–129. [CrossRef]
15. Cai, H.; An, X.; Cui, J.; Li, J.; Wen, S.; Li, K.; Shen, M.; Zheng, L.; Zhang, G.; Shi, X. Facile Hydrothermal Synthesis and Surface Functionalization of Polyethyleneimine-Coated Iron Oxide Nanoparticles for Biomedical Applications. *Mater. Interfaces* **2013**, *5*, 1722–1731. [CrossRef] [PubMed]
16. Veisi, H.; Moradi, S.B.; Saljooqi, A.; Safarimehr, P. Silver Nanoparticle-Decorated on Tannic Acid-Modified Magnetite Nanoparticles (Fe_3O_4@TA/Ag) for Highly Active Catalytic Reduction of 4-Nitrophenol, Rhodamine B and Methylene Blue. *Mater. Sci. Eng. C* **2019**, *100*, 445–452. [CrossRef]
17. Trujillo Hernandez, J.S.; Aragón Muriel, A.; Tabares, J.A.; Pérez Alcázar, G.A.; Bolaños, A. Preparation of Fe_3O_4 nanoparticles and removal of methylene blue through adsorption. *J. Phys. Conf. Ser.* **2015**, *614*, 012007. [CrossRef]
18. Elazab, H.A.; El-Idreesy, T.T. Optimization of the Catalytic Performance of Pd/Fe_3O_4 Nanoparticles Prepared via Microwave-Assisted Synthesis for Pharmaceutical and Catalysis Applications. *Biointerface Res. Appl. Chem.* **2019**, *9*, 3794–3799. [CrossRef]
19. Johnson, C.E.; Johnson, J.A.; Hah, H.Y.; Cole, M.; Gray, S.; Kolesnichenko, V.; Kucheryavy, P.; Goloverda, G. Mössbauer studies of stoichiometry of Fe_3O_4: Characterization of nanoparticles for biomedical applications. *Hyperfine Interact.* **2016**, *237*, 27. [CrossRef]
20. Kamzin, A.S. Mössbauer Investigations of Fe and Fe_3O_4 Magnetic Nanoparticles for Hyperthermia Applications. *Phys. Solid State* **2016**, *58*, 532–539. [CrossRef]
21. Wareppam, B.; Kuzmann, E.; Garg, V.K.; Singh, L.H. Mössbauer spectroscopic investigations on iron oxides and modified nanostructures: A review. *J. Mater. Res.* **2022**, *37*, 1–21. [CrossRef] [PubMed]
22. Hossain, M.; Hossain, M.; Begum, M.; Shahjahan, M.; Islam, M.; Saha, B. Magnetite (Fe_3O_4) Nanoparticles for Chromium Removal. *Bangladesh J. Sci. Ind. Res.* **2018**, *53*, 219–224. [CrossRef]
23. Arévalo, P.; Isasi, J.; Caballero, A.C.; Marco, J.F.; Martín-Hernández, F. Magnetic and Structural Studies of Fe_3O_4 Nanoparticles Synthesized via Coprecipitation and Dispersed in Different Surfactants. *Ceram. Int.* **2017**, *43*, 10333–10340. [CrossRef]
24. Giri, S.K.; Das, N.N.; Pradhan, G.C. Synthesis and Characterization of Magnetite Nanoparticles Using Waste Iron Ore Tailings for Adsorptive Removal of Dyes from Aqueous Solution. *Colloids Surf. A Physicochem. Eng. Asp.* **2011**, *389*, 43–49. [CrossRef]
25. Mikhaylova, M.; Kim, D.K.; Bobrysheva, N.; Osmolowsky, M.; Semenov, V.; Tsakalakos, T.; Muhammed, M. Superparamagnetism of Magnetite Nanoparticles: Dependence on Surface Modification. *Langmuir* **2004**, *20*, 2472–2477. [CrossRef]
26. Yang, C.; Dong, W.; Cui, G.; Zhao, Y.; Shi, X.; Xia, X.; Tang, B.; Wang, W. Highly efficient photocatalytic degradation of methylene blue by P2ABSA-modified TiO_2 nanocomposite due to the photosensitization synergetic effect of TiO_2 and P2ABSA. *RSC Adv.* **2017**, *7*, 23699–23708. [CrossRef]
27. Chen, C.Y.; Liu, Y.R. Robust and Enhanced Photocatalytic Performance of Coupled CdSe/TiO_2 Photocatalysts. *Sci. Adv. Mater.* **2015**, *7*, 1053–1057. [CrossRef]
28. Giovannetti, R.; Rommozzi, E.; D'Amato, C.A.; Zannotti, M. Kinetic Model for Simultaneous Adsorption/Photodegradation Process of Alizarin Red S in Water Solution by Nano-TiO_2 under Visible Light. *Catalysts* **2016**, *6*, 84. [CrossRef]
29. Giovannetti, R.; D' Amato, C.A.; Zannotti, M.; Rommozzi, E.; Gunnella, R.; Minicucci, M.; Di Cicco, A. Visible light photoactivity of Polypropylene coated Nano-TiO_2 for dyes degradation in water. *Sci. Rep.* **2015**, *5*, 17801. [CrossRef]
30. Chen, C.Y.; Hsu, L.J. Kinetic study of self-assembly of Ni(II)-doped TiO_2 nanocatalysts for the photodegradation of azo pollutants. *RSC Adv.* **2015**, *5*, 88266–88271. [CrossRef]

31. Woo, K.; Hong, J.; Choi, S.; Lee, H.; Ahn, J.; Kim, C.S.; Lee, S.W. Easy Synthesis and Magnetic Properties of Iron Oxide Nanoparticles. *Chem. Mater* **2004**, *16*, 2814–2818. [CrossRef]
32. Toby, B.H.; von Dreele, R.B. GSAS-II: The genesis of a modern open-source all purpose crystallography software package. *J. Appl. Cryst.* **2013**, *46*, 544–549. [CrossRef]
33. Varret, F. (University of Le Mans, Le Mans, France); Greneche, J.-M. (University of Le Mans, Le Mans, France). *Unpublished work*, 1994.